Wang and Liu et al.

Compositional transition in natural alkaline lavas through silica-undersaturated melt-lithosphere interaction

Ze-Zhou Wang, Sheng-Ao Liu*, Li-Hui Chen, Shu-Guang Li, and Gang Zeng

***E-mail:** lsa@cugb.edu.cn

This file concludes:

ANALYTICAL METHODS

Zinc isotope ratios were measured at the Isotope Geochemistry Laboratory of the China University of Geosciences, Beijing using the method reported in previous studies (Liu et al., 2014, 2016), which is modified after Maréchal et al. (1999). Before measurement, chemical purification of Zn was conducted. In brief, approximately 10 mg of samples were totally dissolved in an HF-HNO_3 mixture, followed by re-dissolution in aqua regia and 8 N HCl. Afterwards, 1 ml of sample dissolved in 8 N HCl was loaded onto 2 ml pre-cleaned Bio-Rad® strong anion resin AG-MP-1M. Zinc was eluted in 10 ml of 0.5 N HNO_3 after removal of matrix elements, copper and iron rinsed by 8 N HCl and 2 N HCl, respectively. After evaporation to dryness at 80 °C, the residues were dissolved in 1 ml of 3% HNO_3. The Mg/Zn ratio was checked before isotopic measurement since the presence of argides ($Mg^{24}Ar^+$ and $Mg^{26}Ar^+$) significantly influences the ratios of $^{66}Zn/^{64}Zn$ (Mason et al., 2004; Wang et al., 2017). The recovery of Zn is over 99% and the whole procedural blank is less than 6 ng and considered to be negligible compared with the collected Zn (>1 μg).

Zinc isotopic analysis was performed on a Thermo Scientific *Neptune plus* multiple collector inductively coupled plasma mass spectrometry (MC-ICP-MS) instrument using sample-standard bracketing (SSB) method for mass bias correction. The data are reported in δ-notation in per mil relative to JMC 3-0749L Zn standard: $\delta^{68/66}Zn = [(^{68/66}Zn/^{64}Zn)_{sample}/(^{68/66}Zn/^{64}Zn)_{JMC\ 3\text{-}0749L} - 1] \times 1000$. The external reproducibility is ±0.05‰ (2sd) for $\delta^{66}Zn$ and ±0.10‰ (2sd) for $\delta^{68}Zn$

based on long-term analyses of synthetic pure Zn solutions and igneous rock standards. All analyzed samples fall on a mass-dependent fractionation line on a three-isotope plot (δ^{68}Zn vs. δ^{66}Zn) with a slope of 1.979 ± 0.007 (1σ; R^2 = 0.997; N = 60), indicating that there are no analytical artifacts from unresolved isobaric interferences. Analyses of three geostandards going through the same chemical procedures as the studied samples yielded δ^{66}Zn values of 0.34 ± 0.05‰ for BHVO-2, 0.30 ± 0.02‰ for AGV-2 and 0.22 ± 0.03‰ for JP-1, which are consistent with the values reported in the literature (e.g., Sossi et al., 2015; Chen et al., 2016; Wang et al., 2017).

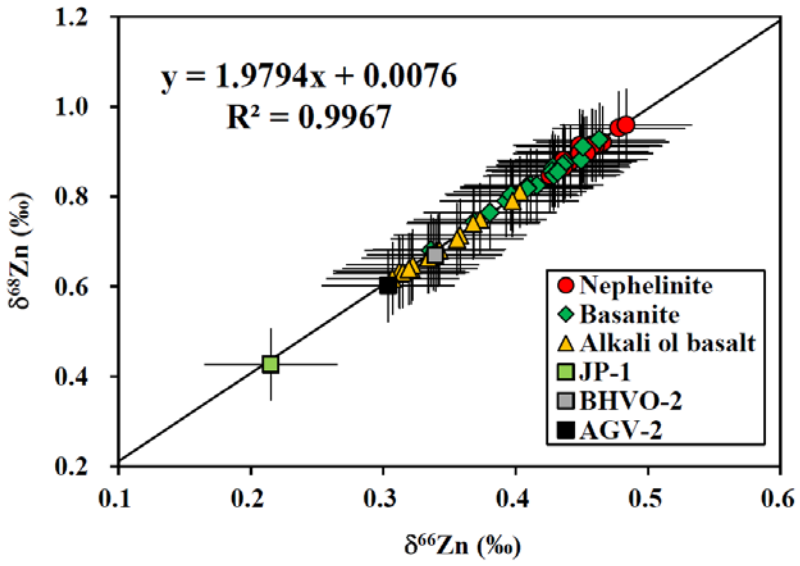

MODEL OF MELT-LITHOSPHERE INTERACTION

Parameters used in the calculation

Name	$\delta^{66}Zn$ (‰)	[Zn] (μg/g)	ε_{Nd}	[Nd] (μg/g)
Basanitic melt[1]	0.45	120	5	40
Orthopyroxene[2]	0.15	30		
SCLM-derived melt[3]	0.23	75	-10	10

[1]Data for basanitic melt are from this study.

[2]Data for orthopyroxene are fromWang et al. (2017).

[3]Zn isotope data for SCLM-derived melt are based on the >120 Ma mafic rocks reported in Liu et al. (2016) and Nd isotope data are based on the data presented in Fig. DR5 (see below).

Melt-opx reaction scenario

The reaction is modelled assuming that peridotite is impregnated by a finite amount of basanitic melt. The equation of melt-opx reaction is 1 $melt^0$ + 0.37 opx → 0.80 $melt^1$ + 0.20 ol + 0.36 cpx (Lambart et al., 2012). $\delta^{66}Zn$ and [Zn] of reacted melt ($melt^1$)can be obtained through the mass balance equation:

$$[Zn]_{melt}^{0} + [Zn]_{opx} \times 0.37 = [Zn]_{melt}^{1} \times 0.80 + [Zn]_{ol} \times 0.20 + [Zn]_{cpx} \times 0.36;$$

$$[Zn]_{melt}^{0} \times \delta^{66}Zn_{melt}^{0} + [Zn]_{opx} \times \delta^{66}Zn_{opx} \times 0.37 = [Zn]_{melt}^{1} \times \delta^{66}Zn_{melt}^{1} \times 0.80 + [Zn]_{ol} \times \delta^{66}Zn_{ol} \times 0.20 + [Zn]_{cpx} \times \delta^{66}Zn_{cpx} \times 0.36;$$

$[Zn]_{ol} / [Zn]_{melt}^{1} \approx D_{Zn}^{ol/melt} = 0.99$, $[Zn]_{cpx} / [Zn]_{melt}^{1} \approx D_{Zn}^{cpx/melt} = 0.48$ (Le Roux et al., 2011; $\delta^{66}Zn_{melt}^{1} = \delta^{66}Zn_{ol} = \delta^{66}Zn_{cpx}$.

Given that f mass fraction of melt participates in the reaction, the final $\delta^{66}Zn$ and [Zn] of the ascending melt after reactive infiltration into the peridotite should be:

$$[Zn]_{final\ melt} = [(1-f) \times [Zn]_{melt}^{0} + f \times [Zn]_{melt}^{1} \times 0.80] / (1-f + f \times 0.80);$$

$\delta^{66}Zn_{final\ melt} = [(1-f) \times [Zn]_{melt}^{0} \times \delta^{66}Zn_{melt}^{0} + f \times [Zn]_{melt}^{1} \times \delta^{66}Zn_{melt}^{1} \times 0.80] / [(1-f) \times [Zn]_{melt}^{0} + f \times [Zn]_{melt}^{1} \times 0.80]$.

Melt-melt mixing scenario

If f proportion of SCLM-derived melt is mixing with the basanitic melt, the $\delta^{66}Zn$ and [Zn] of the mixed melt should be:

$[Zn]_{final\ melt} = ([Zn]_{melt}^{0} \times (1-f) + [Zn]_{SCLM\ melt} \times f)$;

$\delta^{66}Zn_{final\ melt} = (\delta^{66}Zn_{melt}^{0} \times [Zn]_{melt}^{0} \times (1-f) + \delta^{66}Zn_{SCLM\ melt} \times [Zn]_{SCLM\ melt} \times f)/[Zn]_{final\ melt}$.

Similarly, the ε_{Nd} and [Nd] of the mixed melt can also be calculated.

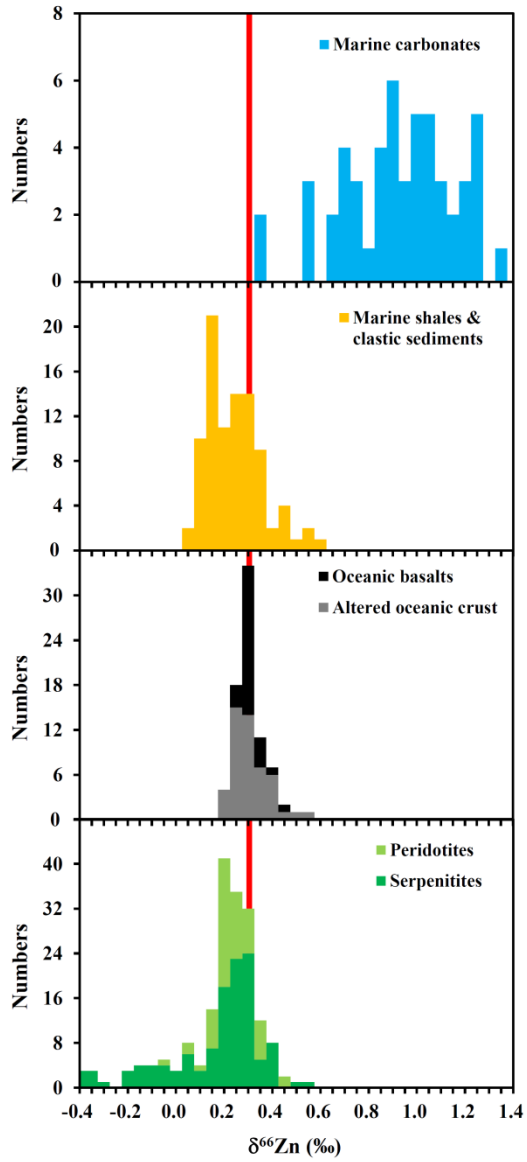

77

78 **Figure DR1.** A compilation of zinc isotope compositions of marine carbonates
79 (Pichat et al., 2003), marine shales and clastic sediments (Bentahila et al., 2008;
80 Pons et al., 2011), oceanic basalts (Herzog et al., 2009; Chen et al., 2013; Wang et
81 al., 2017), altered oceanic crust (Huang et al., 2016), serpentinites (Pons et al., 2011;
82 Pons et al., 2016) and peridotites (Doucet et al., 2016; Wang et al., 2017). The red
83 line refers to the mean value of MORB (Wang et al., 2017).

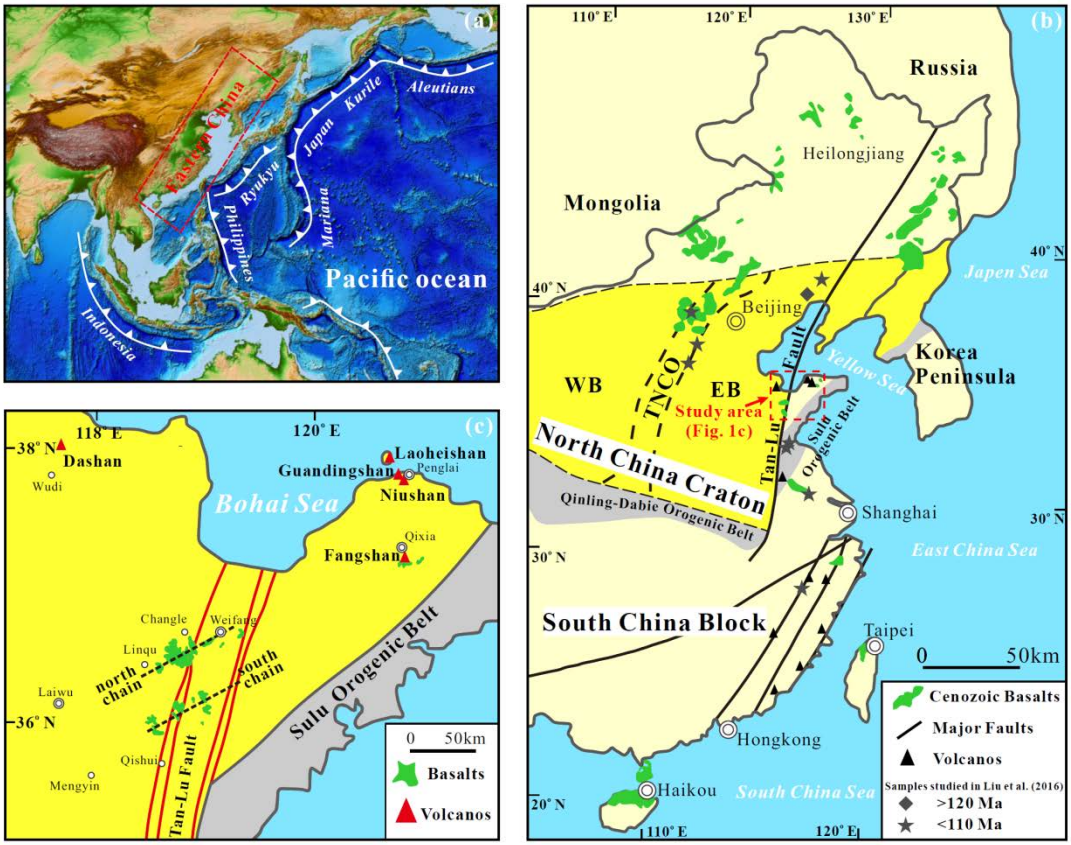

Figure DR2. Schematic maps showing the distribution of Cenozoic alkali basalts in eastern China. (a) Digital topographic map of the western Circum-Pacific region (from http://www.ngdc.noaa.gov/mgg/global/global.html). Distribution of Cenozoic alkali basalts in (b) eastern China and in (c) Shandong Peninsula. Eastern China comprises two major blocks: North China Craton (NCC) and South China Block (SCB), which are separated by the Qinling-Dabie-Sulu orogenic belt. The NCC can be further divided into three parts: Western Block (WB), Eastern Block (EB) and Trans-North China Orogen (TNCO) (Zhao et al., 2001). The Shandong Peninsula is located at the southeastern margin of the EB. Cenozoic alkaline magmatism in Shandong can be divided into two episodes: 24.0-10.3 Ma and 8.7-0.3 Ma (Zeng et al., 2010). The earlier magmatism is mainly located close to the Tan-Lu Fault, which is a deep fault that extends into the lithospheric mantle (e.g., Xu et al., 1987),

97 forming two large parallel volcanic chains: the north chain and the south chain. The
98 later magmatism is widely distributed far from the Tan-Lu Fault in the form of small
99 isolated volcanoes (Fig. 1c) (Zeng et al., 2010, 2011). Locations of samples studied
100 in Liu et al. (2016) are also shown for comparison in Fig. 1b.
101

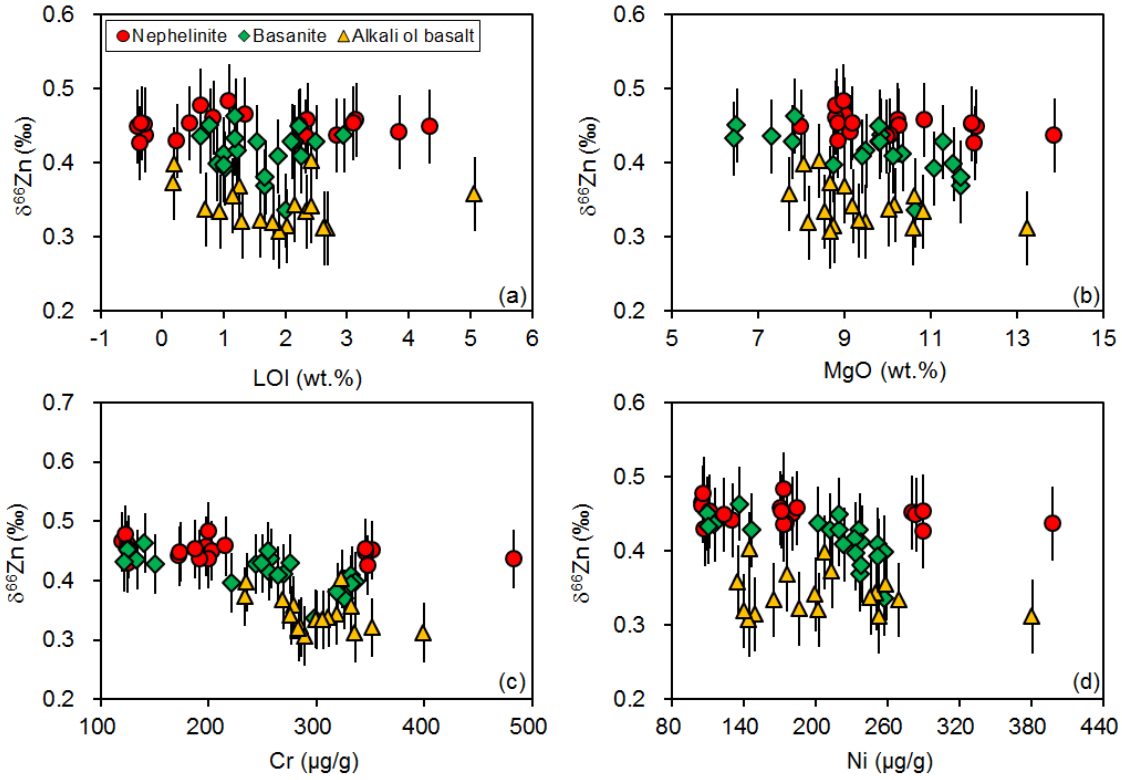

Figure DR3. Plots of $\delta^{66}Zn$ against loss-on-ignition (LOI), MgO, Cr and Ni contents, respectively (a-d). The absence of relationships between $\delta^{66}Zn$ and these elements suggests that post-magmatic alteration and magmatic differentiation have a negligible impact on the Zn isotopic compositions of Shandong alkaline lavas.

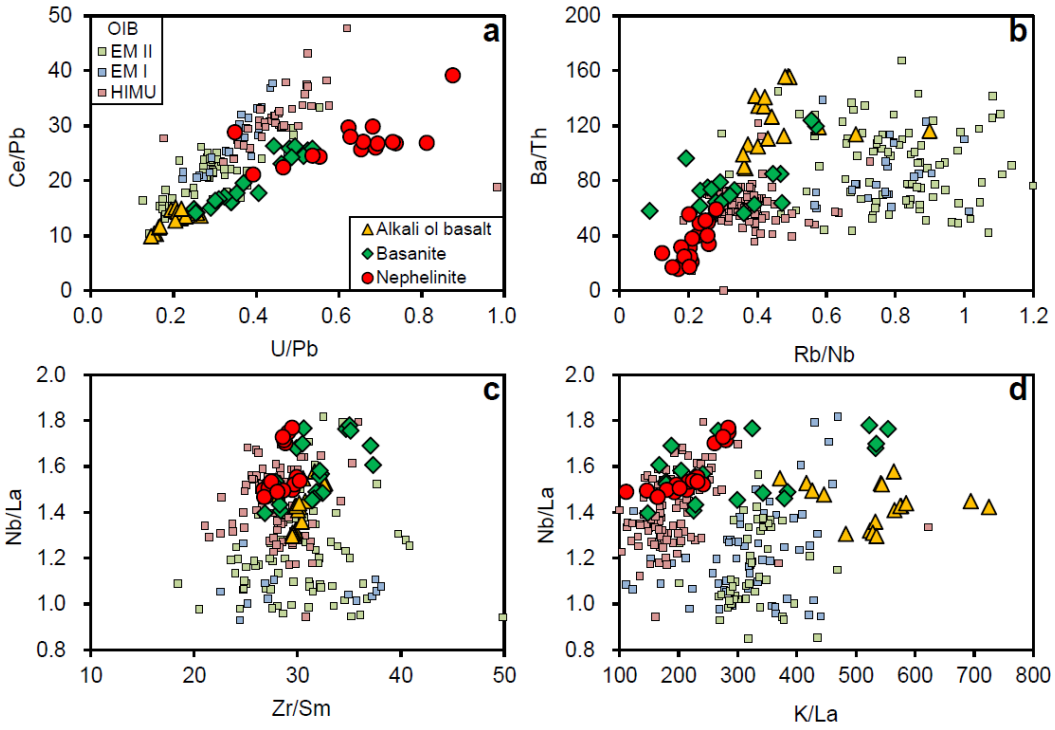

108

109 **Figure DR4. C**omparison of trace elemental ratios between Shandong alkaline lavas

110 and typical HIMU-, EM I- and EM II-type OIBs. (a) Ce/Pb vs. U/Pb; (b) Ba/Th vs.

111 Rb/Nb; (c) Nd/La vs. Zr/Sm; (d) Nb/La vs. K/La. Trace element data of OIBs are

112 from Willbold and Stracke (2006) and those of Shandong alkaline lavas are from

113 Zeng et al. (2010).

114

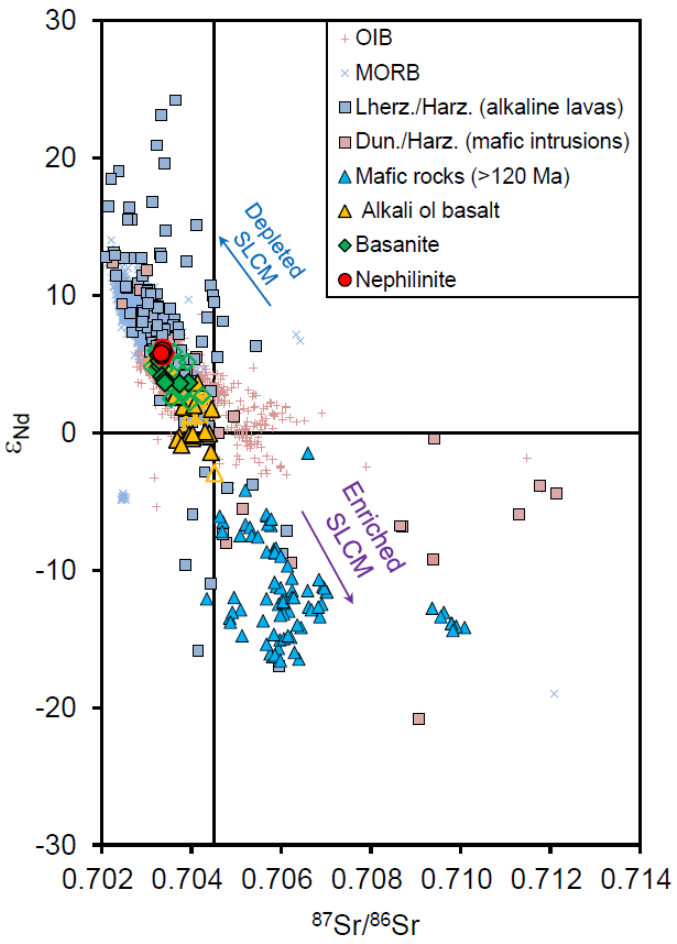

115

116 **Figure DR5.** ε_{Nd} versus $^{87}Sr/^{86}Sr$; Solid colorful symbols represent samples of this
117 study, and open symbols represent samples from other literature (Xu et al., 2012;
118 Sakuyama et al., 2013; Li et al., 2014; Li et al., 2016; Li et al., 2017). Data for OIB
119 and MORB are compiled from GeoRoc (http://georoc.mpch-mainz.gwdg.de/georoc)
120 and PetDB (www.earthchem.org/petdb) respectively. Peridotite xenoliths and > 120
121 Ma mafic rocks are from literature (Song and Frey, 1989; Fan et al., 2000; Zhang et
122 al., 2002; Zhang et al., 2003; Rudnick et al., 2004; Zhang et al., 2004; Tang et al.,
123 2008; Xu et al., 2008a; Xu et al., 2008b; Yang and Li, 2008; Chu et al., 2009; Xiao
124 et al., 2010; Xu et al., 2010; Tang et al., 2011; Zhang et al., 2011; Liu et al., 2012;
125 Tang et al., 2013).

Table DR1. Zinc isotopic compositions (‰), selected element concentrations (major elements in wt. %; trace elements in μg/g), element ratios (w/w) and initial Sr-Nd isotopic ratios for Shandong alkaline lavas.

Sample no.	SiO_2	MgO	Na_2O	K_2O	LOI	Cr	Ni	Zn	Nb	Th	Ce/Pb	Ba/Th	Zn/Fe	La/Yb	$\delta^{66}Zn$	2SD	$\delta^{68}Zn$	2SD	$(^{87}Sr/^{86}Sr)_i$	$\varepsilon_{Nd(t)}$
Nephelinite																				
07JSS01	40.9	12.0	4.7	2.5	1.3	346	290	154	148	10.2	28.0	51.1	14.3	42.3	0.45	0.03	0.90	0.05	0.70336	5.99
07JSS02	40.7	13.9	4.5	2.2	0.8	483	398	149	153	9.7	21.1	59.3	13.9	43.1	0.44	0.03	0.87	0.04	0.70339	5.93
07JSS03	41.1	12.0	4.7	2.4	0.6	348	290	153	147	10	24.6	40.2	14.1	42.8	0.43	0.02	0.85	0.05	0.70334	5.75
07JSS04	40.9	12.0	4.8	2.4	0.2	352	281	154	148	9.8	22.5	34.0	14.1	41.6	0.45	0.04	0.90	0.07	0.70334	5.6
07JSS05	40.9	12.1	4.7	2.4	2.4	346	284	153	147	10.1	24.4	49.8	14.1	41.7	0.45	0.02	0.90	0.03	0.70334	5.75
08LHS01	39.4	8.8	5.5	2.7	0.5	123	107	174	151	13.6	166.3	31.5	15.6	62.8	0.48	0.06	0.95	0.13		
08LHS02	39.5	8.9	5.5	2.7	2.2	126	112	184	146	13.8	120.3	37.9	16.4	63.8	0.45	0.01	0.90	0.04		
08LHS03	39.4	8.9	5.7	2.9	2.8	125	108	176	149	13.6	131.3	49.1	15.7	62.8	0.43	0.04	0.86	0.06		
08LHS04	39.2	9.0	4.7	2.6	3.2	120	106	178	144	13.7	39.2	39.7	15.9	65.7	0.47	0.01	0.92	0.01		
08LHS05	39.4	8.8	4.9	2.7	3.9	126	106	181	132	13.9	29.9	21.0	16.1	64.2	0.46	0.04	0.91	0.07		
08LHS06	39.5	9.2	3.4	1.6	2.3	173	131	169	146	11.9	28.8	24.6	15.8	56.4	0.44	0.03	0.88	0.05		
08LHS07	40.4	8.0	2.9	1.3	3.1	174	124	183	144	13.1	29.7	27.4	16.3	59.5	0.45	0.02	0.91	0.04		
08QJFS01	40.2	9.0	5.2	2.8	1.1	200	174	174	150	15.7	27.1	17.5	16.5	59.5	0.48	0.04	0.96	0.07		
08QJFS02	39.7	9.2	3.4	2.0	4.3	188	172	168	144	15.7	26.8	55.6	16.4	60.2	0.45	0.04	0.90	0.05		
08QJFS03	39.6	10.0	4.1	2.4	-0.3	192	174	172	116	15.6	27.1	24.8	16.6	58.6	0.44	0.03	0.88	0.06		
08QJFS04	39.5	10.3	4.2	2.3	-0.3	198	171	173	119	16.0	26.9	18.2	16.7	57.0	0.5	0.05	0.92	0.09		
08QJFS05	39.5	10.3	4.2	2.3	-0.4	203	181	170	121	16.3	25.7	31.6	16.5	59.0	0.5	0.02	0.90	0.06		
08QJFS06	39.5	10.9	3.7	2.0	-0.3	216	185	167	124	16.5	26.8	17.2	16.5	57.2	0.5	0.02	0.91	0.08		
08QJFS07	39.5	10.1	4.0	2.2	-0.4	200	176	171	120	16.7	26.0	15.8	16.5	59.4	0.4	0.06	0.88	0.04		
Basanite																				

07FS01	43.7	8.8	4.2	1.3	2.5	221	234	110	68	4.6	17.7	73.2	11.4	30.1	0.4	0.05	0.80	0.06	0.70329	5.23
07FS03	43.2	9.5	4.1	0.9	1	256	233	115	66	4.6	19.6	64.5	11.6	31.3	0.42	0.04	0.83	0.07	0.7033	4.86
07FYS07	44.3	10.7	2.8	0.9	3	299	258	100	38	2.3	14.8	96.2	10.8	16.3	0.34	0.02	0.68	0.05	0.70343	5.81
07LIS01	42.8	9.9	3.9	1.0	1.5	258	203	97	75	5.5	17.7	57.9	11.1	29.1	0.44	0.05	0.87	0.04	0.70332	5.15
07LS04	44	10.1	2.6	1.8	1.2	265	224	109	57	4.1	16.6	69.2	12.0	28.7	0.41	0.04	0.82	0.08	0.70341	3.84
07LS05	43.8	9.8	3.1	1.8	1.2	250	220	113	64	4.8	15.0	61.4	12.2	33.3	0.4	0.00	0.85	0.01	0.7034	3.86
07LS06	44.5	9.8	2.9	1.4	1.9	255	220	107	54	3.9	16.4	73.7	11.9	26.6	0.5	0.03	0.88	0.02	0.70341	3.63
07LS07	43.7	9.8	2.8	2.0	0.9	244	213	111	61	4.4	17.1	65.4	12.1	31.2	0.4	0.01	0.86	0.04	0.70335	4.08
07NIS02	44.3	11.7	2.3	1.8	1.0	320	239	97	46	3.2	14.2	123.8	11.1	19.2	0.4	0.04	0.76	0.10	0.70374	3.57
07NIS04	44.2	11.7	2.4	1.8	1.0	326	238	96	46	3.3	14.2	119.7	10.9	19.0	0.4	0.02	0.74	0.04	0.70394	3.63
07THS02	43.6	11.5	3.0	2.3	2.2	336	258	95	59	4.1	16.1	84.8	10.7	21.4	0.4	0.03	0.80	0.04	0.70327	5.64
07THS03	43.7	11.1	2.9	2.2	2.1	332	253	96	61	4.2	16.1	84.8	10.8	21.5	0.4	0.02	0.79	0.02	0.70333	5.77
08GDS01	43	7.8	4.8	2.2	2.3	151	147	160	110	10.6	26.2	75.1	15.8	49.6	0.4	0.03	0.87	0.04		
08GDS02	43.1	7.9	5.0	2.2	1.7	141	137	162	112	10.7	26.3	72.7	16.1	50.1	0.5	0.04	0.93	0.01		
08GDS03	43.4	9.4	4.8	1.3	2.0	333	252	129	96	9.2	24.5	78.8	13.8	41.1	0.4	0.01	0.82	0.05		
08GDS04	41.7	11.3	4.6	1.5	1.7	276	237	127	106	9.5	25.5	51.1	14.2	41.8	0.4	0.03	0.86	0.06		
08GDS05	42.7	10.4	5.3	1.6	0.6	270	239	127	108	9.6	25.8	58.7	13.8	42.1	0.4	0.03	0.83	0.09		
08NIUS01	44.4	7.3	5.6	1.9	2.2	134	116	163	102	9.3	24.2	56.3	16.2	44.2	0.44	0.03	0.87	0.02		
08NIUS02	45	6.5	5.5	1.8	0.8	125	110	163	101	9.1	25.8	62.7	16.1	43.6	0.45	0.01	0.91	0.01		
08NIUS03	45.1	6.5	5.5	1.6	1.2	122	111	160	98	8.7	23.1	63.7	16.3	42.3	0.43	0.03	0.86	0.04		
Alkali olivine basalt																				
07CDS01	45.9	10.6	2.3	1.6	2.6	336	253	94	32	2.1	14.7	134.4	11.3	17.5	0.31	0.02	0.63	0.07	0.70373	-0.29
07CDS02	46.3	10.8	2.2	1.7	2.3	300	270	99	35	2.4	13.9	126.5	11.6	18.5	0.33	0.03	0.66	0.06	0.70397	-0.18
07CDS03	45.4	13.3	1.7	1.3	2.7	399	381	92	30	1.9	13.2	89.1	10.8	15.6	0.31	0.06	0.63	0.12		
07CDS04	46	7.7	1.9	1.5	5.1	279	135	89	33	2.2	15.1	134.1	11.5	17.3	0.36	0.03	0.71	0.06	0.70402	-0.41
07CDS05	47.1	9.5	2.7	1.5	1.3	352	203	93	31	2.0	14.4	141.7	11.3	16.9	0.32	0.01	0.64	0.01	0.70369	-0.51

07CDS07	47.6	8.6	2.7	1.6	0.9	306	166	92	32	2.2	14.9	140.7	11.0	17.0	0.33	0.05	0.66	0.03	0.70378	-0.9
07FYS01	47.4	8.8	2.5	1.4	2	284	150	92	28	1.8	11.5	155.8	11.4	14.5	0.31	0.03	0.63	0.07	0.70396	-0.2
07FYS02	47.6	8.2	2.7	1.5	1.8	284	141	93	29	1.9	11.7	155.7	11.4	14.4	0.32	0.03	0.64	0.04	0.70404	-0.1
07FYS03	47.6	8.7	2.5	1.4	1.9	289	145	91	28	1.8	11.5	155.5	11.3	14.7	0.31	0.05	0.62	0.03	0.70396	-0.16
07FYS04	46.4	9.2	2.6	1.5	2.4	276	200	106	44	3.2	13.6	105.1	12.2	22.4	0.34	0.07	0.68	0.12	0.70382	1.89
07FYS06	46	8.4	2.6	1.5	2.4	324	145	91	50	3.4	13.7	106.4	11.7	25.0	0.4	0.01	0.81	0.03	0.70414	3.63
07FYS09	47.4	9.0	2.5	1.5	1.3	269	177	95	41	2.9	13.5	112.6	11.6	18.7	0.37	0.00	0.74	0.00	0.70446	1.72
07FYS10	47.2	9.4	2.5	1.4	1.6	286	187	94	41	2.9	13.5	110.5	11.4	18.3	0.32	0.04	0.65	0.01	0.70406	2.01
07LIS02	46.9	8.7	3.5	2.0	0.2	234	214	103	46	3.2	14.2	90.4	11.8	22.3	0.37	0.01	0.75	0.07	0.70361	2.57
07LIS04	47.5	8.1	3.5	2.0	0.2	236	208	105	46	3.2	12.7	99.0	11.8	22.3	0.4	0.03	0.79	0.06	0.70363	2.65
07SW01	47.4	10.0	2.8	1.6	0.7	311	246	101	26	2.2	10.4	113.7	11.6	12.9	0.34	0.01	0.67	0.00	0.70431	0.06
07SW02	47	10.2	2.5	1.6	2.2	319	251	100	27	2.2	10.3	116.2	11.6	13.2	0.34	0.02	0.68	0.03	0.7044	-0.06
07SW03	47.4	10.6	2.6	1.2	1.2	332	259	101	24	2.1	9.9	118.9	11.6	12.6	0.36	0.04	0.71	0.08	0.70444	-1.42
Rock standards																				
JP-1															0.22	0.03	0.43	0.01		
BHVO-2															0.34	0.05	0.67	0.08		
AGV-2															0.3	0.02	0.6	0.06		

The data of major-trace elemental concentrations and Sr-Nd isotopic ratios are from Zeng et al. (2010, 2011). 2SD refers to two standard deviations of the population of three repeat runs of the same solution.

REFERENCES CITED

Bentahila, Y., Othman, D. B., and Luck, J.-M., 2008, Strontium, lead and zinc isotopes in marine cores as tracers of sedimentary provenance: A case study around Taiwan orogen: Chemical Geology, v. 248, no. 1, p. 62-82, doi:10.1016/j.chemgeo.2007.10.024.

Chen, H., Savage, P. S., Teng, F.-Z., Helz, R. T., and Moynier, F., 2013, Zinc isotope fractionation during magmatic differentiation and the isotopic composition of the bulk Earth: Earth and Planetary Science Letters, v. 369, p. 34-42, doi:10.1016/j.epsl.2013.02.037.

Chen, S., Liu, Y., Hu, J., Zhang, Z., Hou, Z., Huang, F., and Yu, H., 2016, Zinc isotopic compositions of NIST SRM 683 and whole-rock reference materials: Geostandards and Geoanalytical Research, v. 40, no. 3, p. 417-432, doi:10.1111/j.1751-908X.2015.00377.x.

Chu, Z.-Y., Wu, F.-Y., Walker, R. J., Rudnick, R. L., Pitcher, L., Puchtel, I. S., Yang, Y.-H., and Wilde, S. A., 2009, Temporal evolution of the lithospheric mantle beneath the eastern North China Craton: Journal of Petrology, v. 50, no. 10, p. 1857-1898, doi:10.1093/petrology/egp055.

Doucet, L. S., Mattielli, N., Ionov, D. A., Debouge, W., and Golovin, A. V., 2016, Zn isotopic heterogeneity in the mantle: A melting control?: Earth and Planetary Science Letters, v. 451, p. 232-240, doi:10.1016/j.epsl.2016.06.040.

Fan, W., Zhang, H., Baker, J., Jarvis, K., Mason, P., and Menzies, M., 2000, On and off the North China Craton: where is the Archaean keel?: Journal of Petrology, v. 41, no. 7, p. 933-950, doi:10.1093/petrology/41.7.933.

Herzog, G., Moynier, F., Albarède, F., and Berezhnoy, A., 2009, Isotopic and elemental abundances of copper and zinc in lunar samples, Zagami, Pele's hairs, and a terrestrial basalt: Geochimica et Cosmochimica Acta, v. 73, no. 19, p. 5884-5904, doi:10.1016/j.gca.2009.05.067.

Huang, J., Liu, S. A., Gao, Y., Xiao, Y., and Chen, S., 2016, Copper and zinc isotope systematics of altered oceanic crust at IODP Site 1256 in the eastern equatorial Pacific: Journal of Geophysical Research: Solid Earth, v. 121, no. 10, p. 7086-7100, doi:10.1002/2016JB013095.

Lambart, S., Laporte, D., Provost, A., and Schiano, P., 2012, Fate of pyroxenite-derived melts in the peridotitic mantle: thermodynamic and experimental constraints: Journal of Petrology, v. 53, no. 3, p. 451-476, doi:10.1093/petrology/egr068.

Le Roux, V., Dasgupta, R., and Lee, C.-T., 2011, Mineralogical heterogeneities in the Earth's mantle: Constraints from Mn, Co, Ni and Zn partitioning during partial melting: Earth and Planetary Science Letters, v. 307, no. 3, p. 395-408, doi:10.1016/j.epsl.2011.05.014.

Li, H.-Y., Huang, X.-L., and Guo, H., 2014, Geochemistry of Cenozoic basalts from the Bohai Bay Basin: Implications for a heterogeneous mantle source and lithospheric evolution beneath the eastern North China Craton: Lithos, v. 196, p. 54-66, doi:10.1016/j.lithos.2014.02.026.

Li, H.-Y., Xu, Y.-G., Ryan, J. G., Huang, X.-L., Ren, Z.-Y., Guo, H., and Ning, Z.-G., 2016, Olivine and melt inclusion chemical constraints on the source of intracontinental basalts from the eastern North China Craton: Discrimination of contributions from the subducted Pacific slab: Geochimica et Cosmochimica Acta, v. 178, p. 1-19, doi:10.1016/j.gca.2015.12.032.

Li, H. Y., Xu, Y. G., Ryan, J. G., and Whattam, S. A., 2017, Evolution of the mantle beneath the eastern North China Craton during the Cenozoic: Linking geochemical and geophysical observations: Journal of Geophysical Research: Solid Earth, v. 122, no. 1, p. 224-246, doi:10.1002/2016JB013486. 2.

Liu, J., Carlson, R. W., Rudnick, R. L., Walker, R. J., Gao, S., and Wu, F.-y., 2012, Comparative Sr-Nd-Hf-Os-Pb isotope systematics of xenolithic peridotites from

Yangyuan, North China Craton: additional evidence for a Paleoproterozoic age: Chemical Geology, v. 332, p. 1-14, doi:10.1016/j.chemgeo.2012.09.013.
Liu, S.-A., Li, D., Li, S., Teng, F.-Z., Ke, S., He, Y., and Lu, Y., 2014, High-precision copper and iron isotope analysis of igneous rock standards by MC-ICP-MS: Journal of Analytical Atomic Spectrometry, v. 29, no. 1, p. 122-133, doi:10.1039/C3JA50232E.
Liu, S.-A., Wang, Z.-Z., Li, S.-G., Huang, J., and Yang, W., 2016, Zinc isotope evidence for a large-scale carbonated mantle beneath eastern China: Earth and Planetary Science Letters, v. 444, p. 169-178, doi:10.1016/j.epsl.2016.03.051.
Maréchal, C. N., Télouk, P., and Albarède, F., 1999, Precise analysis of copper and zinc isotopic compositions by plasma-source mass spectrometry: Chemical Geology, v. 156, no. 1, p. 251-273, doi:10.1016/S0009-2541(98)00191-0.
Mason, T. F., Weiss, D. J., Horstwood, M., Parrish, R. R., Russell, S. S., Mullane, E., and Coles, B. J., 2004, High-precision Cu and Zn isotope analysis by plasma source mass spectrometry Part 1. Spectral interferences and their correction: Journal of Analytical Atomic Spectrometry, v. 19, no. 2, p. 209-217, doi:10.1039/B306958C.
Pichat, S., Douchet, C., and Albarède, F., 2003, Zinc isotope variations in deep-sea carbonates from the eastern equatorial Pacific over the last 175 ka: Earth and Planetary Science Letters, v. 210, no. 1, p. 167-178, doi:10.1016/S0012-821X(03)00106-7.
Pons, M.-L., Debret, B., Bouilhol, P., Delacour, A., and Williams, H., 2016, Zinc isotope evidence for sulfate-rich fluid transfer across subduction zones: Nature communications, v. 7, p. 13794, doi:10.1038/ncomms13794.
Pons, M.-L., Quitté, G., Fujii, T., Rosing, M. T., Reynard, B., Moynier, F., Douchet, C., and Albarède, F., 2011, Early Archean serpentine mud volcanoes at Isua, Greenland, as a niche for early life: Proceedings of the National Academy of Sciences, v. 108, no. 43, p. 17639-17643, doi:10.1073/pnas.1108061108.
Rudnick, R. L., Gao, S., Ling, W.-L., Liu, Y.-S., and McDonough, W. F., 2004, Petrology and geochemistry of spinel peridotite xenoliths from Hannuoba and Qixia, North China craton: Lithos, v. 77, no. 1, p. 609-637, doi:10.1016/j.lithos.2004.03.033.
Sakuyama, T., Tian, W., Kimura, J.-I., Fukao, Y., Hirahara, Y., Takahashi, T., Senda, R., Chang, Q., Miyazaki, T., and Obayashi, M., 2013, Melting of dehydrated oceanic crust from the stagnant slab and of the hydrated mantle transition zone: Constraints from Cenozoic alkaline basalts in eastern China: Chemical Geology, v. 359, p. 32-48, doi:10.1016/j.chemgeo.2013.09.012.
Song, Y., and Frey, F. A., 1989, Geochemistry of peridotite xenoliths in basalt from Hannuoba, eastern China: implications for subcontinental mantle heterogeneity: Geochimica et Cosmochimica Acta, v. 53, no. 1, p. 97-113, doi:10.1016/0016-7037(89)90276-7.
Sossi, P. A., Halverson, G. P., Nebel, O., and Eggins, S. M., 2015, Combined separation of Cu, Fe and Zn from rock matrices and improved analytical protocols for stable isotope determination: Geostandards and Geoanalytical Research, v. 39, no. 2, p. 129-149, doi:10.1111/j.1751-908X.2014.00298.x.
Tang, Y.-J., Zhang, H.-F., Nakamura, E., and Ying, J.-F., 2011, Multistage melt/fluid-peridotite interactions in the refertilized lithospheric mantle beneath the North China Craton: constraints from the Li-Sr-Nd isotopic disequilibrium between minerals of peridotite xenoliths: Contributions to Mineralogy and Petrology, v. 161, no. 6, p. 845-861, doi:10.1007/s00410-010-0568-1.
Tang, Y.-J., Zhang, H.-F., Ying, J.-F., Su, B.-X., Chu, Z.-Y., Xiao, Y., and Zhao, X.-M., 2013, Highly heterogeneous lithospheric mantle beneath the Central Zone of the North China Craton evolved from Archean mantle through diverse melt refertilization: Gondwana Research, v. 23, no. 1, p. 130-140, doi:10.1016/j.gr.2012.01.006.
Tang, Y.-J., Zhang, H.-F., Ying, J.-F., Zhang, J., and Liu, X.-M., 2008, Refertilization of ancient lithospheric mantle beneath the central North China Craton: evidence from petrology and geochemistry of peridotite xenoliths: Lithos, v. 101, no. 3, p. 435-452, doi:10.1016/j.lithos.2007.09.006.
Wang, Z.-Z., Liu, S.-A., Liu, J., Huang, J., Xiao, Y., Chu, Z.-Y., Zhao, X.-M., and Tang, L., 2017, Zinc isotope fractionation during mantle melting and constraints on the Zn

isotope composition of Earth's upper mantle: Geochimica et Cosmochimica Acta, v. 198, p. 151-167, doi:10.1016/j.gca.2016.11.014.

Willbold, M., and Stracke, A., 2006, Trace element composition of mantle end‐members: Implications for recycling of oceanic and upper and lower continental crust: Geochemistry, Geophysics, Geosystems, v. 7, no. 4, doi:10.1029/2005GC001005.

Xiao, Y., Zhang, H.-F., Fan, W.-M., Ying, J.-F., Zhang, J., Zhao, X.-M., and Su, B.-X., 2010, Evolution of lithospheric mantle beneath the Tan-Lu fault zone, eastern North China Craton: evidence from petrology and geochemistry of peridotite xenoliths: Lithos, v. 117, no. 1, p. 229-246, doi:10.1016/j.lithos.2010.02.017.

Xu, J., Zhu, G., Tong, W., Cui, K., and Liu, Q., 1987, Formation and evolution of the Tancheng-Lujiang wrench fault system: a major shear system to the northwest of the Pacific Ocean: Tectonophysics, v. 134, no. 4, p. 273-310, doi:10.1016/0040-1951(87)90342-8.

Xu, W., Hergt, J. M., Gao, S., Pei, F., Wang, W., and Yang, D., 2008a, Interaction of adakitic melt-peridotite: implications for the high-Mg# signature of Mesozoic adakitic rocks in the eastern North China Craton: Earth and Planetary Science Letters, v. 265, no. 1, p. 123-137, doi:10.1016/j.epsl.2007.09.041.

Xu, W., Yang, D., Gao, S., Pei, F., and Yu, Y., 2010, Geochemistry of peridotite xenoliths in Early Cretaceous high-Mg# diorites from the Central Orogenic Block of the North China Craton: the nature of Mesozoic lithospheric mantle and constraints on lithospheric thinning: Chemical Geology, v. 270, no. 1, p. 257-273, doi:10.1016/j.chemgeo.2009.12.006.

Xu, Y.-G., Blusztajn, J., Ma, J.-L., Suzuki, K., Liu, J.-F., and Hart, S. R., 2008b, Late Archean to Early Proterozoic lithospheric mantle beneath the western North China craton: Sr-Nd-Os isotopes of peridotite xenoliths from Yangyuan and Fansi: Lithos, v. 102, no. 1, p. 25-42, doi:10.1016/j.lithos.2007.04.005.

Xu, Z., Zhao, Z.-F., and Zheng, Y.-F., 2012, Slab–mantle interaction for thinning of cratonic lithospheric mantle in North China: geochemical evidence from Cenozoic continental basalts in central Shandong: Lithos, v. 146, p. 202-217, doi:10.1016/j.lithos.2012.05.019.

Yang, W., and Li, S., 2008, Geochronology and geochemistry of the Mesozoic volcanic rocks in Western Liaoning: implications for lithospheric thinning of the North China Craton: Lithos, v. 102, no. 1, p. 88-117, doi:10.1016/j.lithos.2007.09.018.

Zeng, G., Chen, L.-H., Hofmann, A. W., Jiang, S.-Y., and Xu, X.-S., 2011, Crust recycling in the sources of two parallel volcanic chains in Shandong, North China: Earth and Planetary Science Letters, v. 302, no. 3, p. 359-368, doi:10.1016/j.epsl.2010.12.026.

Zeng, G., Chen, L.-H., Xu, X.-S., Jiang, S.-Y., and Hofmann, A. W., 2010, Carbonated mantle sources for Cenozoic intra-plate alkaline basalts in Shandong, North China: Chemical Geology, v. 273, no. 1, p. 35-45, doi:10.1016/j.chemgeo.2010.02.009.

Zhang, H.-F., Sun, M., Zhou, M.-F., Fan, W.-M., Zhou, X.-H., and Zhai, M.-G., 2004, Highly heterogeneous Late Mesozoic lithospheric mantle beneath the North China Craton: evidence from Sr-Nd-Pb isotopic systematics of mafic igneous rocks: Geological Magazine, v. 141, no. 1, p. 55-62, doi:10.1017/S0016756803008331.

Zhang, H.-F., Sun, M., Zhou, X.-H., Fan, W.-M., Zhai, M.-G., and Yin, J.-F., 2002, Mesozoic lithosphere destruction beneath the North China Craton: evidence from major-, trace-element and Sr-Nd-Pb isotope studies of Fangcheng basalts: Contributions to Mineralogy and Petrology, v. 144, no. 2, p. 241-254, doi:10.1007/s00410-002-0395-0.

Zhang, H.-F., Sun, M., Zhou, X.-H., Zhou, M.-F., Fan, W.-M., and Zheng, J.-P., 2003, Secular evolution of the lithosphere beneath the eastern North China Craton: evidence from Mesozoic basalts and high-Mg andesites: Geochimica et Cosmochimica Acta, v. 67, no. 22, p. 4373-4387, doi:10.1016/S0016-7037(03)00377-6.

Zhang, J., Zhang, H., Kita, N., Shimoda, G., Morishita, Y., Ying, J., and Tang, Y., 2011, Secular evolution of the lithospheric mantle beneath the eastern North China craton: evidence from peridotitic xenoliths from Late Cretaceous mafic rocks in the Jiaodong region, east-central China: International Geology Review, v. 53, no. 2, p. 182-211,

doi:10.1080/00206810903025090.
Zhao, G., Wilde, S. A., Cawood, P. A., and Sun, M., 2001, Archean blocks and their boundaries in the North China Craton: lithological, geochemical, structural and P-T path constraints and tectonic evolution: Precambrian Research, v. 107, no. 1, p. 45-73, doi:10.1016/S0301-9268(00)00154-6.